University of Groningen

Modelling of cross-flow membrane contactors

Dindore, V. Y.; Brilman, D. W. F.; Versteeg, G. F.

IMPORTANT NOTE: You are advised to consult the publisher's version (publisher's PDF) if you wish to cite from it. Please check the document version below.

Document Version
Publisher's PDF, also known as Version of record

Publication date:
2005

Link to publication in University of Groningen/UMCG research database

Modelling of cross-flow membrane contactors: Mass transfer with chemical reactions

V.Y. Dindore [a,*], D.W.F. Brilman [b], G.F. Versteeg [a]

[a] *Design and Development of Industrial Processes, Faculty of Chemical Technology, University of Twente,*
P.O. Box 217, 7500 AE Enschede, The Netherlands
[b] *Sasol Technology Netherlands B.V., Hallenweg 5, 7522 NB Enschede, The Netherlands*

Abstract

Conventionally, carbon dioxide and hydrogen sulphide are absorbed using aqueous alkanolamines or carbonate solution in column type of equipment. However, in view of the unparallel advantages offered, the use of microporous hollow fiber membrane modules is an attractive alternative. In the present study application of cross-flow membrane contactors for absorption of these gases using aqueous potassium carbonate as a solvent is explored. The carbon dioxide and hydrogen sulphide absorption into aqueous solutions carbonate involves complex chemical reactions. The effect of these chemical reactions on the absorption into a liquid flowing though a hollow fiber membrane may not be described using conventional mass transfer models like e.g. the penetration or surface renewal model due to the lack of a well defined liquid phase bulk and the presence of a laminar velocity profile in the mass transfer zone. Moreover, in the case of cross-flow membrane contactors, the concentrations of both fluids, inside and outside the fibers, vary in both directions i.e. in the direction of flow and in the direction normal to the flow. Hence the theoretical analysis of the cross-flow membrane contactor is more complicated. To describe the effect of the chemical reaction on the absorption rate in the cross-flow hollow fiber contactor, a detailed mathematical model was developed using first principles. A complete scheme of the reversible ionic reactions and equilibria involved was implemented in the model to describe the solute uptake. The experiments were carried out study the effects various parameters such as gas and liquid velocities, bulk concentrations of solute gas and liquid phase reactant. The theoretical predictions were compared with experimental results. An excellent match between experimental results and model predictions was obtained.
© 2005 Elsevier B.V. All rights reserved.

Keywords: Hollow fiber membranes; Membrane contactors; Gas treating; Cross-flow; Modelling

1. Introduction

Natural gas, refinery gas contains hydrogen sulphide as a major impurity. Hydrogen sulphide is a highly toxic and corrosive gas and considered as one of the major sources for the environmental problems such as acid rains. Therefore, in order to utilize these fuels for chemical processing or energy generation, the hydrogen sulphide concentration in these gases must be reduced to very low levels; less than $0.0115 \, \text{g/m}^3$ is required for certain specific applications [32].

* Corresponding author. Present address: NTNU, Institute for Kjemisk Processteknologi, K-5, N-7491 Trondheim, Norway. Tel.: +47 73594598; fax: +47 73594080.
E-mail address: vishwas.dindore@chemeng.ntnu.no (V.Y. Dindore).

Increasing demand of energy has given more attention to the low quality natural gas containing high percentages of carbon dioxide (up to 30%). In view of high transportation cost and corrosive effects caused by carbon dioxide, it is necessary to reduce the concentration of carbon dioxide to acceptable levels. Typically 2% carbon dioxide is stipulated as a pipeline specification. Carbon dioxide is also produced whenever fossil fuels such as natural gas or coal are burned for energy generation. A typical rate of carbon dioxide generation from a thermal power plant is $5 \times 10^5 \, \text{kg/h}$ in the case of 600 MW coal fired plant. Emission of carbon dioxide is regarded as a serious potential cause for environmental problems such as global warming. Hence, carbon dioxide capture from these sources is important if the green house effect is to be reduced.

The most common process for removal of these gases is an absorption into a solvent using conventional gas–liquid contactors such as packed or plate column. Both hydrogen sulphide and carbon dioxide are acidic in nature and are similar in many physical and chemical aspects. Hence, the solvents used for the removal of carbon dioxide in gas treating process also absorb hydrogen sulphide. Compared to physical solvents, enhanced absorption incorporating chemical reaction results into high selectivity and reduced solvent circulation. Therefore, there has been great deal of effort in applying chemical solvents such as aqueous solutions of alkanolamines and aqueous carbonate solutions. In addition to the conventional absorption processes utilizing column type of contactors, the use of microporous hollow fiber membrane contactors is an attractive alternative. In view of the unparallel advantages offered by these hollow fiber membrane contactors, considerable academic and industrial work has been done to develop these contactors for natural gas treating [11]. However, up to now only very few of these processes have been successfully tested on a larger scale. Kvaerner Oil and Gas and W.L. Gore and Associates GmbH have been developing a membrane gas absorption process for the removal of acid gases from natural gas and exhausts of the offshore gas turbines [16]. In this process, PTFE hollow fiber membranes are used in combination with physical (Morphysorb®) or chemical (alkanolamines) solvents. However, PTFE hollow fibers are not available in small diameters (few hundred microns) and are more expensive, making natural gas treating using membrane gas absorption not so attractive as compared to the conventional absorption process. TNO Environment Energy and Process Innovation (the Netherlands) have been developing a membrane gas absorption process for the removal of CO_2 from flue gases using commercially available and cheaper polypropylene hollow fiber membranes. However, the conventional alkanolamine solutions are found to wet the polypropylene membranes. To avoid these wetting problems, TNO has developed a range of new reactive absorption liquids based on the amino acid salt solutions [15]. Nevertheless, these newly developed reactive solvent may suffer from the problem of precipitation of reaction products at high amine concentration and high amine loading [21]. The precipitation of the reaction products may result into a significant increase in the overall mass transfer resistance due to the blockage of the membrane pores.

On the other hand, absorption of carbon dioxide and hydrogen sulphide into aqueous carbonate solutions using polyolefin membranes contactors has been studied experimentally by Nii et al. [24] and Chun and Lee [5] who found that modules made up of polyolefin membranes are ideally suitable for this system. However, the theoretical analysis of this system is more difficult due to complex reactions involved in the system. These investigators used an overall mass transfer coefficient or simple kinetics to describe the system. The more detailed theoretical analysis of carbon dioxide absorption into potassium carbonate system using membrane contactors by Lee et al. [22] lacks experimental validation of the system.

It is important to note that all the work was carried out using parallel-flow modules, where the change in the concentration of shell-side fluid is uni-axial (i.e. along the axis of module or in the direction of flow). In case of cross-flow membrane contactors the concentrations of both fluids vary significantly in both directions i.e. in the direction of flow as well as in the direction normal to the flow and thus the change is bi-axial for both fluids. Hence the theoretical analysis of cross-flow membrane contactor is more complex.
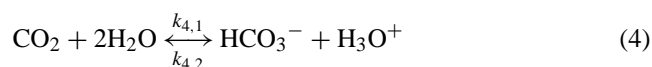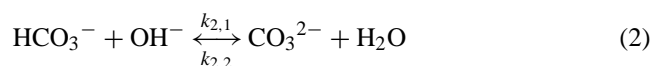
In this work, a detailed theoretical analysis is carried out for the removal of carbon dioxide and hydrogen sulphide by absorption into aqueous potassium carbonate solutions using cross-flow hollow fiber membrane contactors. Complete reversible reactions scheme was included in the microscopic theoretical model equations as opposed to the use of overall mass transfer coefficient to describe solute uptake. The theoretical predictions were validated by the experimental analysis carried out using commercial as well as laboratory-made cross-flow membrane contactors.

2. Theory: mass transfer with chemical reactions

2.1. Reactive absorption of carbon dioxide in aqueous carbonate solutions

Absorption of carbon dioxide into the aqueous carbonate solutions has been studied by many investigators [17,30,31]. In these studies most of the work has been carried out using high bicarbonate to the carbonate ratios. In such cases the carbon dioxide into the aqueous carbonate buffer solutions can be treated as absorption accompanied by an irreversible pseudo-first order reaction. The chemical absorption mechanism under the conditions of low or negligible bicarbonate to carbonate ratio is, however, more complex and contains two-step reversible reactions [34].

When the potassium carbonate is dissolved in water it is ionized into the potassium ion (K^+) and carbonate ion (CO_3^{2-}). The bicarbonate ion (HCO_3^-) and hydroxyl ion (OH^-) are then generated by the inverse of reaction 2 in following reaction scheme. The various reactions taking place during the absorption of carbon dioxide into the aqueous potassium carbonate solution are given below [17].

$$CO_2 + OH^- \underset{k_{1,2}}{\overset{k_{1,1}}{\longleftrightarrow}} HCO_3^- \tag{1}$$

$$HCO_3^- + OH^- \underset{k_{2,2}}{\overset{k_{2,1}}{\longleftrightarrow}} CO_3^{2-} + H_2O \tag{2}$$

$$2H_2O \underset{k_{3,2}}{\overset{k_{3,1}}{\longleftrightarrow}} H_3O^+ + OH^- \tag{3}$$

$$CO_2 + 2H_2O \underset{k_{4,2}}{\overset{k_{4,1}}{\longleftrightarrow}} HCO_3^- + H_3O^+ \tag{4}$$

$$CO_2 + CO_3^{2-} + H_2O \leftrightarrow 2HCO_3^- \tag{5}$$

Reactions (1) and (4) are rate controlling reactions [17,30]. Reaction (1) is practically irreversible for the pH values greater than 10. Reaction (4) is much slower and only of importance in solutions with pH values less than 8 [25]. The reactions (2) and (3) involve only proton transfer and can be considered as instantaneous so that they can be assumed to be at equilibrium [17]. Reaction (5) is the overall reaction of carbon dioxide absorption in aqueous carbonate solution. The corresponding equilibrium constants of the reactions are defined as follows:

$$K_1 = \frac{[HCO_3^-]}{[CO_2][OH^-]} \tag{6}$$

$$K_2 = \frac{[CO_3^{2-}]}{[HCO_3^-][OH^-]} \tag{7}$$

$$K_w = [H_3O^+][OH^-] \tag{8}$$

$$K_4 = \frac{[HCO_3^-][H_3O^+]}{[CO_2]} \tag{9}$$

All the kinetic parameters can be obtained from the literature and are given in Appendix A. The initial bulk concentration of each species can be determined by simultaneously solving the equilibrium equations along with a mass balance for the carbon species and an electro-neutrality balance.

$$K_1 A_0 B_0 - C_0 = 0 \tag{10a}$$

$$K_2 B_0 C_0 - E_0 = 0 \tag{10b}$$
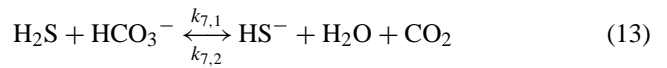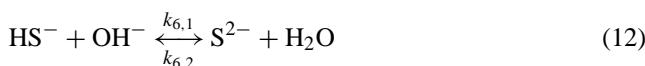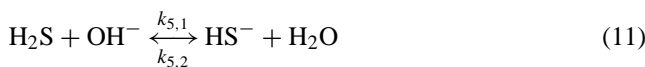
$$E_{ini} - A_0 - C_0 - E_0 = 0 \tag{10c}$$

$$H_3O^+ - \frac{K_w}{B_0} = 0 \tag{10d}$$

$$K^+ + H_3O^+ = B_0 + C_0 + 2E_0 \tag{10e}$$

where $A = CO_2$, $B = OH^-$, $C = HCO_3^-$ and $E = CO_3^{2-}$. E_{ini} refers to the initial concentration of the K_2CO_3. In the implementation of the complete numerical model, the initial concentrations were calculated using Newton's method. These solutions were reported to be non-ideal solutions, the effect of non-ideality was taken into account in the form of ionic strength and its effect on various kinetic and equilibrium constants (refer Appendix A).

2.2. Reactive absorption of hydrogen sulphide in aqueous carbonate solutions

Once the hydrogen sulphide is physically absorbed into the aqueous carbonate solution following reactions take place along with reactions (2) and (3).

$$H_2S + OH^- \underset{k_{5,2}}{\overset{k_{5,1}}{\rightleftarrows}} HS^- + H_2O \tag{11}$$

$$HS^- + OH^- \underset{k_{6,2}}{\overset{k_{6,1}}{\rightleftarrows}} S^{2-} + H_2O \tag{12}$$

$$H_2S + HCO_3^- \underset{k_{7,2}}{\overset{k_{7,1}}{\rightleftarrows}} HS^- + H_2O + CO_2 \tag{13}$$

$$H_2S + CO_3^{2-} \leftrightarrow HS^- + HCO_3^- \tag{14}$$

Reaction (11) is extremely fast and is very much favored to the right. The reaction (12) has an equilibrium constant of $0.12\,m^3\,kmol^{-1}$ at $25\,^\circ C$ at infinite dilution [2], hence reaction (12) is of minor importance in the strongly alkaline solutions and can be entirely neglected in the weakly alkaline solutions such as aqueous carbonate solution. The final result of the reaction (13) is the production of carbon dioxide, which should desorb into the gaseous phase if no carbon dioxide is present in the gaseous phase. Reaction (13) is made up of two steps; reaction (11) followed by inverse of reaction (1). The second step of reaction (13) is non-ionic and rate determining and has a very low kinetic rate constant [1]. Hence reaction (13) can be neglected in comparison with overall reaction. Eq. (14) gives the overall reaction of hydrogen sulphide in aqueous carbonate solution with above assumptions and equilibrium for this reaction is favored to the right (equilibrium constant of 2×10^3 at $25\,^\circ C$). Initial bulk concentrations of carbonate, bicarbonate and hydroxyl ions can be calculated by simultaneously solving the set of equations (10). All the kinetic parameters in this reaction scheme can be obtained from the literature and are given in Appendix A.

3. Model development

Numerous mass transfer models such as film, penetration and surface renewal models are available in literature to describe the reactive absorption of a gas in a liquid. The basic and common assumption of all these models is the presence of a well-mixed bulk phase adjacent to the gas–liquid interface. For the present case of the reactive absorption of a gas in a liquid flowing through a hollow fiber, this well-mixed liquid bulk, however, is absent. Due to the laminar flow of liquid through the hollow fiber, there is a velocity profile in the liquid phase which extends from the gas–liquid interface to the axis of the fiber. Hence, the mathematical treatment of the present problem to predict the absorption rate and mass transfer coefficient in the presence of chemical reactions is not straightforward. However, for physical absorption and constant gas–liquid interface conditions, Kreulen et al. [20] proposed an approximate solution for the mass transfer coefficient analogous to the heat transfer coefficient in the constant wall temperature heat transfer problem of Graetz [12] and Leveque [23].

$$\text{For } Gz < 10, \qquad Sh = 3.67 \tag{15a}$$

$$\text{For } Gz > 20, \qquad Sh = 1.62(Gz)^{1/3} \tag{15b}$$

$$\text{For } 10 < Gz < 20, \qquad Sh = \sqrt[3]{3.67^3 + 1.62^3 Gz} \tag{15c}$$

The above equation was found applicable for the complete range of Graetz numbers in the laminar flow regime.

Nevertheless, due to the limitations mentioned above the mass transfer process involving chemical reaction in the liquid flowing through the hollow fiber has to be described by a model based on first principles. The fiber side mass balance for a species 'i' was derived from the equation of continuity and is given by,

$$V_z \frac{\partial C_i}{\partial z} = D_i \left[\frac{1}{r} \frac{\partial}{\partial r} \left(r \frac{\partial C_i}{\partial r} \right) \right] - R_i \tag{16}$$

where 'R' is the source term due to the chemical reaction. The adiabatic temperature rise during the absorption process was considered to be negligible. The assumption is valid in the present case, since the absorption flux in a fiber was very low. In addition, the length of fiber used in the module was considerably small. The change in the interface temperature due to the absorption can also be neglected since the solubility of the gas is low [10]. As the liquid flow inside the fiber was laminar, the velocity profile in the radial direction is given by,

$$V_z = 2\bar{v} \left[1 - \left(\frac{r}{r_{\text{in}}} \right)^2 \right] \tag{17}$$

The entrance effects had been neglected as the liquid flows through the hollow fiber for a considerable distance ($>10d_{\text{in}}$, required for the velocity profile to be fully developed, [26]) before it contacts the gas phase. A generalized reversible reaction scheme to take into account the multiple reactions, as described in Sections 2.1 and 2.2, was incorporated in the model. The set of partial differential Eq. (16) requires one initial condition and two boundary conditions in the axial and radial directions for each component, respectively. For the axial direction, the inlet conditions/properties of the components are specified.

$$\text{At } z = 0, \quad C_i = C_{i,o} \quad (0 \leq r \leq r_{\text{in}}) \tag{18}$$

In the radial direction, symmetry was assumed at the axis of the cylindrical fiber,

$$\text{At } r = 0, \quad \left(\frac{\partial C_i}{\partial r} \right) = 0 \quad (0 \leq z \leq L) \tag{19}$$

At the gas–liquid interface, the conservation of mass with respect to the component 'A' that is absorbed from the gas phase was enforced.

$$\text{At } r = r_{\text{in}}, \quad D_A \left(\frac{\partial C_A}{\partial r} \right) = k_{\text{ext}}(C_{A,g} - C_{A,g,i})$$

$$(0 \leq z \leq L) \tag{20}$$

All components other than the gas species absorbed were assumed to be non-volatile.

$$\text{At } r = r_{\text{in}}, \quad \left(\frac{\partial C_i}{\partial r} \right) = 0 \quad (0 \leq z \leq L) \tag{21}$$

In case of the cross-flow membrane contactors, the shell side concentration of the solute as well as the volumetric flow rate of the gas changes in both directions. This effect is significant when the concentration of the solute in the gas stream is substantial and the fraction removed in the membrane contactor is relatively high. To take this effect into account the shell-side flow was divided into number of cells. The details of the cell arrangement are presented elsewhere [8]. A dispersive mixing between the adjacent cells in the direction normal to the shell-side flow was considered. The shell side dispersion coefficients, in the direction of flow and in the direction normal to the flow, were determined in separate experiments using RTD analysis. The details of these RTD experiments and results are presented elsewhere and are used in this study [9]. This method preserves concentration gradient of gas and liquid phase in all directions. A solute balance over a single cell (m, n) gives following equation.

$$Q_{Gm-1,n} C_{Gm-1,n} - Q_{Gm,n} C_{Gm,n} = A_{m,n} J_{m,n} \tag{22}$$

Based on this mass balance for a single cell the solute outlet concentration and the gas outlet flow rate were calculated for every cell by an iterative method. The gas concentration, gas flow rate and liquid concentration were assumed to be uniform at the inlet of the module. The composition and gas flow rate leaving the last row of cells were stored and were used as inputs for the corresponding cells in the next row.

The set of equations (the number depending on the number of chemical species involved in the reaction scheme) on the fiber side and on the shell side was solved simultaneously using a numerical technique. The details of the numerical treatment are given in Section 4. The solution of the mass balance equations results into the concentration profile of the solute in the liquid as well as gas phase. Based on these concentration profiles, the local absorption flux of the solute along the length of the fiber was calculated using Fick's law for each cell. The average solute absorption flux over the entire module was obtained by integrating local flux over the complete module. The change in the driving force in the cross-flow contactors results into the concentration profile in the outlets of the contactor. The final outlet concentrations were computed by mixing the different outlet streams and by taking the mixing cup concentration.

4. Numerical treatment

In the case of gas absorption in a liquid flowing through a hollow fiber, the mass transfer rate was calculated from the concentration profiles were species along the radius and the length of the fiber. The concentration profiles were obtained as a solution of a system of non-linear parabolic partial differential equations subjected to specified initial and boundary conditions. These concentration profiles are steep near the gas–liquid interface when absorption is follow by a chemical reaction. In order to have a finer grid near the gas–liquid interface, the distribution of spatial grid points in the r–z plane was transformed. The final set of the partial differen-

tial equation was discretised using the implicit second order scheme based on the Baker and Oliphant method [3]. The reaction terms were linearised using the Newton–Raphson method. The discretization for 'np' grid point in radial direction gives a set of np + 1 equation for each component at each z-directional grid point. These equations were solved simultaneously using LU decomposition method according to Crout algorithm. This solution was used to calculate the set of equations at the next z-directional coordinate.

5. Experimental

5.1. Materials

The potassium carbonate salt, carbon dioxide, hydrogen sulphide and nitrogen used in the experiments were of 99.99% purity. Owing to commercial availability and the high hydrophobic nature of polypropylene as a membrane material, it was decided to use an Accurel Q3/2 polypropylene hollow fiber for module construction. The Q3/2 fiber has an outside diameter meter of 1000 μm and inside diameter of 600 μm. The maximum pore size of the Q3/2 fiber is 0.64 μm. Two modules were used in the experiments. The details of the modules are given in Table 1.

Module I was obtained from TNO-MEP, Apeldoorn, the Netherlands and module II was constructed in our laboratory. The details of construction of module II are given elsewhere [8]. Fig. 1a and b shows the cross-flow modules I and II. In both modules, the length of the potting was more than 5 cm. This ensures that the potting length on the liquid entry side provides sufficient distance ($>10d_{in}$) for the laminar liquid flow profile inside the fiber to be fully developed, before it contacts the gas. Uniform flow distribution on the shell side is important to prevent maldistribution and dead zone formation. To achieve the uniform flow distribution on the shell, the shell side fluid was passed through an area reducer filled with glass wool.

5.2. Method

Absorption of carbon dioxide into aqueous potassium carbonate was carried out in module II. The experimental set-up for the carbon dioxide absorption is shown in Fig. 2. A continuous mode of gas–liquid contacting operation was used during the experiments. Aqueous potassium carbonate solutions were prepared by dissolving a known amount potassium carbonate salt into the degassed and deionized water. The carbonate solution was passed through the fibers and gas
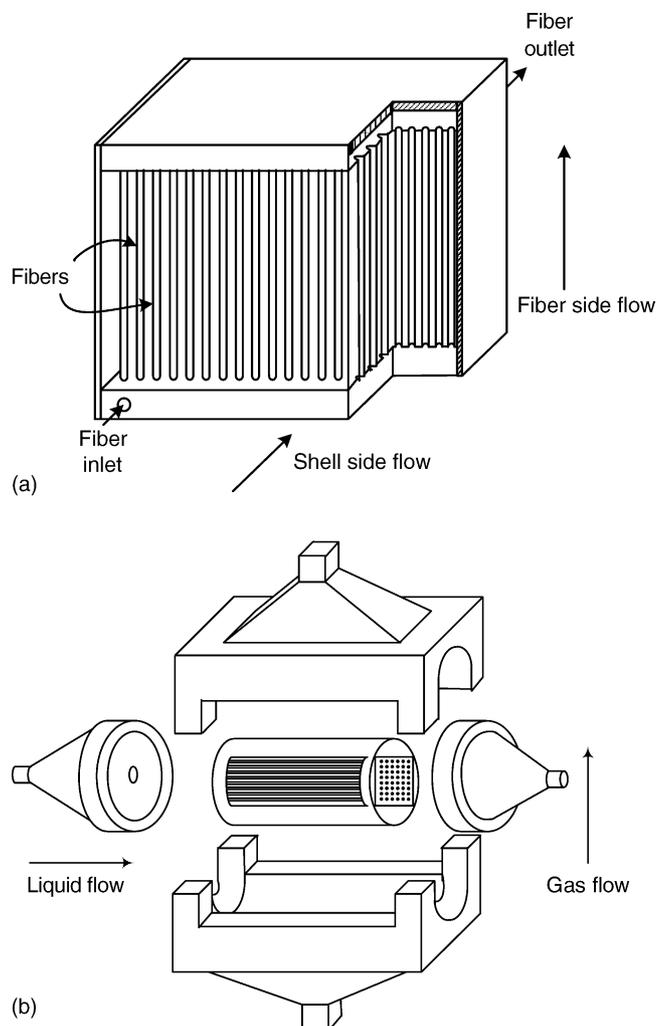

Fig. 1. Cross-flow membrane modules I (a) and II (b).

was passed through the shell-side. The carbonate solution was fed using a gear-pressure pump through the heat exchanger to maintain the desired temperature before passing to the hollow fiber membrane module. The upstream liquid pressure was controlled using a high precision back-pressure controller valve. In all experiments, sufficient gas pressure was maintained in the contactor before starting the liquid flow as the absence of the gas pressure may result in the wetting of the fiber. The liquid inlet and liquid outlet pressures were measured separately using digital pressure indicators. The liquid inlet was also fitted with a digital thermometer to monitor the liquid inlet temperature. The average velocity of the liquid through the fibers was measured by collecting a calibrated amount of sample in a fixed period of time.

Table 1
Module specifications

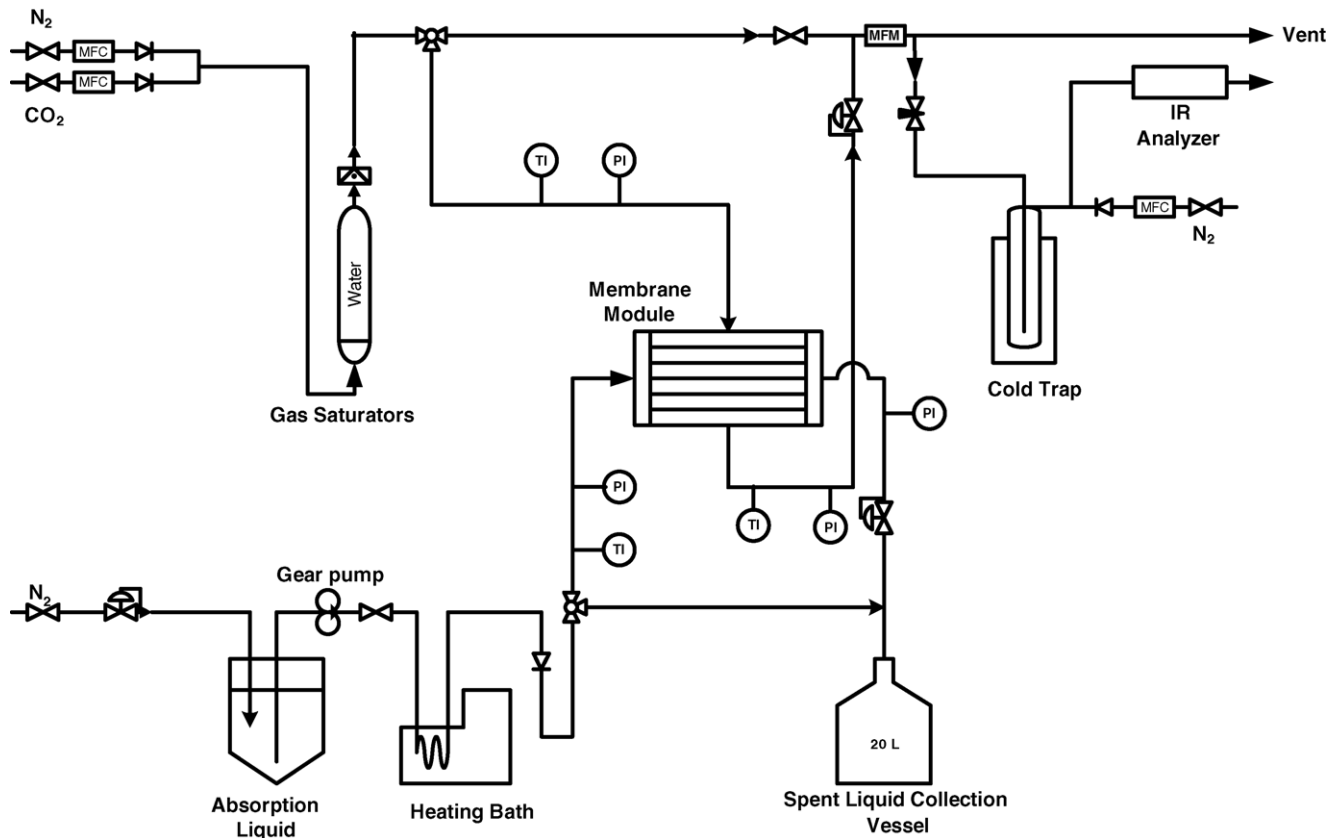| Module	Fiber type	Length (m)	Width (m)	Height (m)	Number of fibers	Voidage	Pitch	A_{in} (m^2)
I	PP	0.05	0.05	0.05	729	0.77	1.85	0.069
II	PP	0.1	0.04	0.04	400	0.80	2.0	0.074

Fig. 2. Experimental set-up for absorption of CO_2 in aqueous K_2CO_3 solution.

The shell-side gas flow was adjusted using mass flow controllers. All mass flow controllers were calibrated using a gas flow meter or soap film meter. Nitrogen and carbon dioxide were premixed to a desired concentration using mass flow controllers and fed to the contactor after saturating the gas stream with water vapor. The shell-side pressure was controlled using a 5866-Brooks digital pressure controller. During all the experiments the liquid side pressure was kept sufficiently higher than the shell side gas pressure to avoid the bubbling of gas. The gas inlet and gas outlet pressure were measured separately using digital pressure indicators. The gas inlet and outlet were also equipped with digital thermometers to monitor the temperatures. It is important to know both inlet and outlet temperatures of the gas stream in order to check any cooling effect which might result into a change in the volumetric gas flow rate. The carbon dioxide concentration in the feed and outlet gas streams of the contactor was measured using Maihak Infrared carbon dioxide analyzers of different ranges depending on gas composition (0–5%, 0–15%). The concentrations of the gas samples to the infrared (IR) analyzer were adjusted within the range of the IR analyzer by diluting the gas stream with nitrogen. The carbon dioxide absorption flux and liquid average outlet concentration was estimated by making a mass balance over the reactor.

$$\langle J_{CO_2} \rangle = \frac{Q_{G,i}C_{G,i} - Q_{G,e}C_{G,e}}{A} \qquad (23)$$

$$C_{L,e} = \frac{Q_{G,i}C_{G,i} - Q_{G,e}C_{G,e}}{Q_L} \qquad (24)$$

Since the infrared analyzer gives carbon dioxide concentrations in terms of volume percentage, it was possible to calculate both the volumetric gas flow rate and the molar concentration of carbon dioxide using the overall mass balance. In all experiments the gas flow rate was kept sufficiently low so that the outlet gas flow rate and molar concentration of the carbon dioxide was significantly lower than the inlet conditions. All the experiments were carried out at atmospheric pressure and 24.0 °C.

Absorption of hydrogen sulphide into aqueous potassium carbonate solution was carried out in a separate experimental set-up at TNO-MEP laboratory. The details of the experimental set-up are given in Fig. 3. The experiments were carried out using a stack of four modules (type I) arranged to realise an overall counter-current operation. The carbonate solution was recirculated over the membrane absorber through the fiber. The water lost due to the evaporation was made up in the storage vessel. The liquid-circulation loop was equipped with temperature and pressure indicators at the inlet and the outlet of the stream. The pH of the solution was continuously monitored using a pH-meter. The liquid velocity through the hollow fiber was calculated by measuring the total liquid flow fed to the membrane absorber. All the experiments were carried out at atmospheric pressure and 20.0 °C.
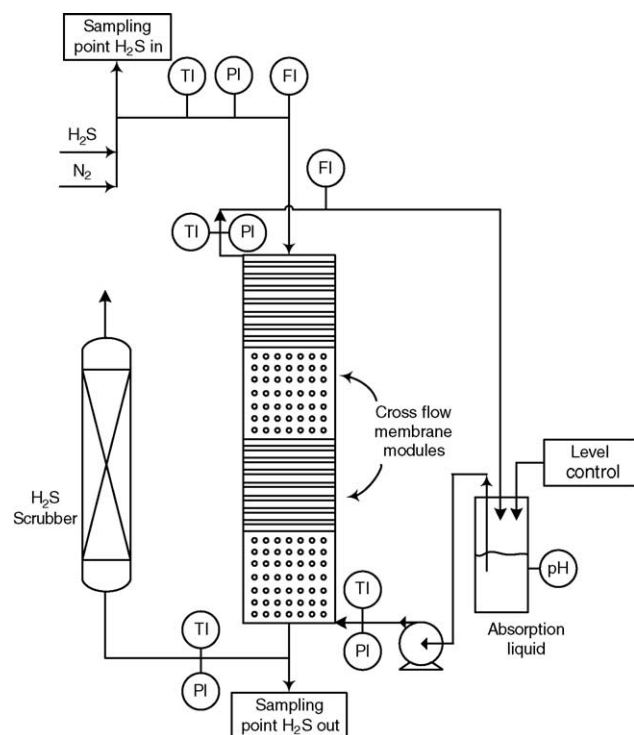
Fig. 3. Experimental set-up for absorption of H$_2$S in aqueous K$_2$CO$_3$ solution.

Hydrogen sulphide was premixed with nitrogen to obtain a gas stream with the desired hydrogen sulphide concentration. This gas stream was fed continuously through the membrane absorber. For safety reasons, a hydrogen sulphide scrubber was installed after the membrane gas absorption unit to remove completely the traces of hydrogen sulphide before it was passed to the vent. The gas-circulation loop was also equipped with temperature and pressure indicators to measure the inlet and outlet temperatures and pressures. The concentration of hydrogen sulphide in the inlet and outlet stream was measured using a Galvanic H$_2$S analyzer. As the liquid was continuously recirculated over the module, the liquid was continuously loaded with hydrogen sulphide till it got completely saturated with hydrogen sulphide. At this point there was no absorption of hydrogen sulphide as the gas and liquid streams reached equilibrium and this resulted into the same level of concentrations for inlet and outlet gas-streams. To simulate the once through experiments for both gas as well as liquid, the outlet concentration at $t = 0$ was taken as outlet concentration at zero loading of hydrogen sulphide.

6. Results and discussion

In case of mass transfer with chemical reaction in membrane gas–liquid contactors, the overall mass transfer resistance can be controlled by either of gas film resistance, membrane resistance or liquid side resistance depending on the enhancement due to chemical reaction. Hence informa-

tion on the gas side (shell-side in present case) mass transfer coefficient and membrane mass transfer coefficient is necessary. Jansen et al. [14] studied the shell side mass transfer performance of the cross-flow rectangular module similar to those used in this study. The shell side mass transfer coefficient for these modules was given by the following equation.

$$Sh = 0.9 Re^{0.5} Sc^{0.33} \tag{25}$$

The membrane mass transfer coefficient becomes a key factor for the gas film controlled systems such as absorption of H$_2$S into alkalis and carbonate solutions. Qi and Cussler [28] reported an overall gas phase and membrane mass transfer coefficient of 0.0073 m/s for the absorption of H$_2$S into NaOH, which is considerably lower than that for the conventional gas–liquid contactors. In these situations, the absorption of such system is strongly influenced by the membrane mass transfer coefficient. The membrane mass transfer coefficient depends on the structural properties of the membrane such as porosity to tortuosity ratio (ε/τ), Knudsen diffusion parameter (K_o) and viscous flow parameter (B_o). To determine these parameters separate gas permeation experiments were carried out. The details of these experiments and results are given in Appendix B. The membrane mass transfer coefficient was calculated by the method described by Dindore et al. [7]. The estimated value of the membrane mass transfer coefficient was 1.9×10^{-2} m s^{-1}. Once the individual mass transfer coefficients are known, the combined mass transfer coefficient of the gas phase and the membrane phase was calculated by the resistance in series model.

The diffusivity of carbon dioxide in water was obtained from literature [35] and diffusivity of hydrogen sulphide in water was estimated using the correlation given by Diaz et al. [6]. Ion diffusivities of the simple ions in water at infinite dilution were estimated using the Nerst equation. These diffusivities were corrected using the Stokes–Einstein relation for the viscosity changes of the solutions. Electro-neutrality in the liquid phase was maintained by using mean ion diffusion coefficients for the ionic species in the liquid phase. Solubilities of carbon dioxide and hydrogen sulfide in water as a function of temperature were obtained from literature and these data were corrected for the ionic strength of the solution using the method given by Weisenberger and Schumpe [36]. All the parameters used in the model simulation are given in Appendix A.

6.1. Absorption of carbon dioxide in aqueous carbonate solutions

Absorption of carbon dioxide into 0.25 and 0.5 M aqueous carbonate solutions was carried out using Module II. The experiments were carried out to study the effects of various operating parameters such as liquid velocity, gas velocity and concentration of the aqueous carbonate solution. In all experiments the gas residence time in the membrane module was kept high enough to ensure a significant change in the gas
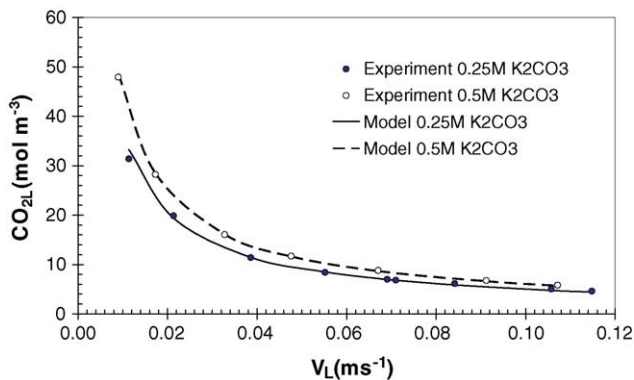
Fig. 4. Effect of liquid velocity on the liquid outlet concentration for the absorption of carbon dioxide in module II.

Fig. 6. Effect of liquid velocity on the average absorption flux in module II.

phase concentration. All the experiments were carried out using 32.63% (15.86 mol m^{-3}) carbon dioxide.

Fig. 4 shows the carbon dioxide concentration in the liquid outlet stream as a function of the liquid velocity through the fibers and subsequent comparison with the numerical model predictions. Note that the carbon dioxide concentration is given as total carbon dioxide present in the form of physically dissolved carbon dioxide as well as in the form of reaction products. It can be seen from the figure that the numerical predictions are in good agreement with the experimental results. No fit parameters were used in the numerical simulations. As expected, the carbon dioxide concentration decreases as the liquid flow rate increases. The effect of the concentration of carbonate solution is also shown in the figure. It can be seen from the figure that as the concentration of the carbonate solution is increased, the concentration of the absorbed carbon dioxide is also increased. This indicates that the increase in the concentration of carbonate ions results into the increase in carbon dioxide absorption in line with Eq. (5).

Fig. 5 shows the gas outlet concentration as a function of liquid velocity through the fibers for a constant gas inlet flow rate of 0.42 and 0.55 l min^{-1} for 0.25 and 0.5 M K$_2$CO$_3$ solution, respectively. It can be seen from the figure that as the liquid velocity increases the gas outlet concentration of
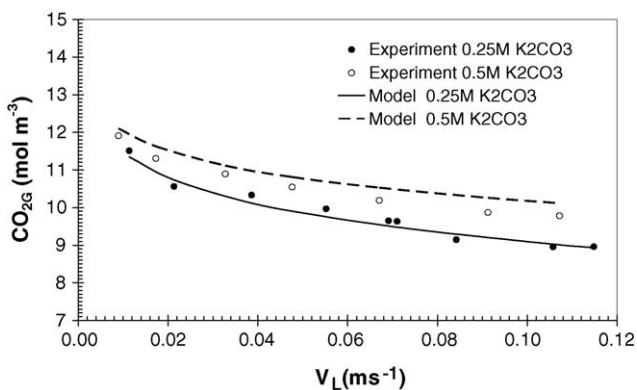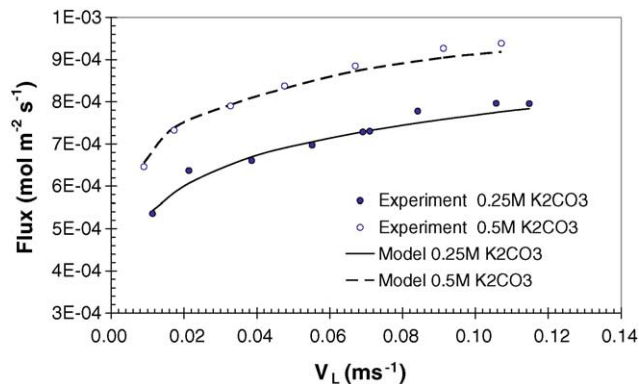
carbon dioxide decreases. This indicates the increase in the removal rate of carbon dioxide with the liquid flow rate.

The effect of the liquid velocity on the average absorption flux is shown in Fig. 6. The average absorption flux in the module was calculated by integrating the local absorption flux over the entire volume of the module. It can be seen from the figure that the absorption flux is a strong function of the liquid velocity when the liquid velocity is relatively low. However, at higher velocities the average absorption flux is less dependent on the liquid velocity. It is known from the theory of mass transfer with chemical reaction that in the case of fast reaction regime the absorption flux is independent of the mass transfer coefficient whereas in the case of instantaneous reaction regime the absorption flux depends on the mass transfer coefficient. In the present case of gas absorption accompanied with chemical reaction into a liquid flowing through hollow fiber, there is relatively less depletion of the reactive species at the gas–liquid interface over the entire length of fiber at higher liquid velocities. This situation resembles to the fast reaction regime. Therefore in this case the absorption rate is dominated by the chemical reaction rate and the liquid velocity has less influence on the average absorption flux. However, at lower velocities significant depletion of the reactive species may occur. For extreme case of the complete depletion of the reactive species at the interface, the reaction regime may change from fast reaction regime at the liquid inlet to instantaneous reaction regime at liquid exit. In such cases the absorption rate is limited by the radial diffusion of reacting species to the reaction plane and the flux is strongly influenced by the mass transfer coefficient and hence by the liquid velocity. In the case of cross-flow membrane contactor, the solute gas concentration on the shell side also decreases in the direction of the gas flow. Higher depletion of the solute gas in the direction of the gas flow results into change in reaction regime in the direction of gas flow as well. Thus in the case of cross-flow membrane contactor, the reaction regime changes along length of fiber as well as in the direction of the gas flow. Therefore the application of conventional mass transfer models for complete module becomes difficult and detailed mathematical modelling of the contactor is necessary.

Fig. 5. Effect of liquid velocity on the gas outlet concentration for the absorption of carbon dioxide in module II.
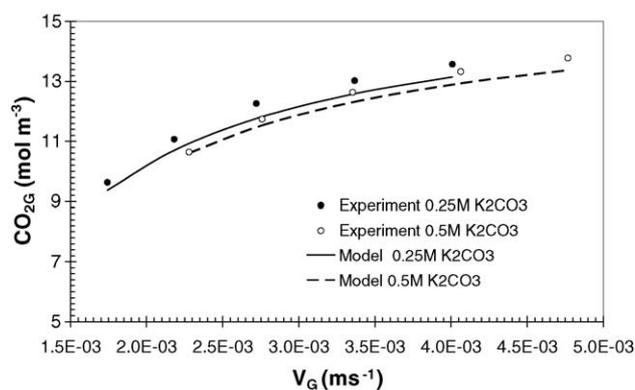
Fig. 7. Effect of gas velocity on the gas outlet concentration for the absorption of carbon dioxide in module II.

The effect of gas velocity on the gas outlet concentration and average absorption flux in module is shown in Figs. 7 and 8, respectively. The experiments were carried out at constant liquid velocity at 0.06 m s^{-1}. As can be seen from Fig. 7, the gas outlet concentrations predicted by the simulation are in good agreement with the experiment results. Fig. 8 indicates that average absorption flux in the module is less dependent on the gas velocity. It can be concluded that the overall mass transfer process for the absorption of carbon dioxide into aqueous carbonate solutions using hollow fiber membrane contactor is still controlled by the liquid side mass transfer resistance even after enhancement due to chemical reaction.
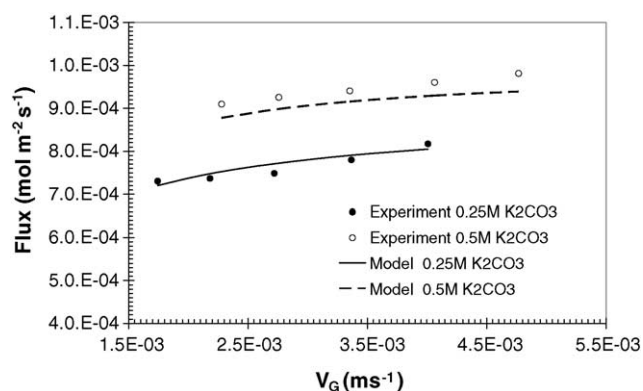

Fig. 8. Effect of gas velocity on the absorption flux for the absorption of carbon dioxide in module II.

6.2. Absorption of hydrogen sulphide in aqueous carbonate solutions

The absorption of hydrogen sulphide was carried out using a stack of four modules of type I in TNO-MEP laboratories. The experiments were carried out in such a mode that overall counter current flow was realized. Experiments were carried out for two different gas velocities 0.556 and 1.11 m s^{-1}, respectively. The liquid velocity through the fiber was kept

Table 2
Experimental conditions for H$_2$S absorption

Variable	Value
Temperature (°C)	20
Pressure (bar)	1
Inlet H$_2$S concentration (ppm)	93–2071
K$_2$CO$_3$ concentration (kmol m^{-3})	0.2–2
Liquid velocity (m s^{-1})	2.69×10^{-3}
Gas velocity (m s^{-1})	0.556–1.11

constant for all the experiments (2.69×10^{-3} m s^{-1}). The experimental conditions are given in Table 2.

Throughout an experiment the carbonate solution gets loaded with the hydrogen sulphide from the feed gas due to continuous recirculation of the solvent and thus hydrogen sulphide loading of carbonate solution steadily increases with time. The absorption flux of the hydrogen sulphide drops steadily due to increase in the back-pressure of the hydrogen sulphide. As a consequence, the outlet gas stream concentration of the hydrogen sulphide increases steadily with time. The temporal variation of hydrogen sulphide loading of carbonate solution and the outlet gas stream concentration of the hydrogen sulphide for a typical case is shown in Fig. 9. It can be seen from the figure that after a certain period of time, the outlet gas stream concentration becomes identical to the inlet gas stream concentration. The summary of the experimental results is given in Table 3.

The numerical simulations were carried out for the stack of modules using the experimental data. In all the experiments the outlet concentration of the hydrogen sulphide was measured as function of time. However, the model simulations were carried out for steady-state operation for once through experiments. Hence to compare the results of the simulations and experiments, the outlet concentration measured at time $t = 0$ was taken as the result for a once through experiment. In the experiment, the outlet of one module was passed as a single inlet for the next module in the stack. In actual model simulations, a uniform concentration in the inlet streams would result in a concentration gradient (and flow gradient as well for the gas stream) in the streams leaving the final segment
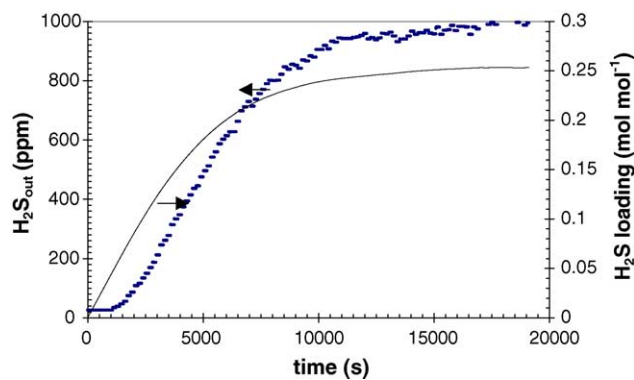

Fig. 9. H$_2$S concentration at the gas outlet and H$_2$S loading as a function of time (gas inlet concentration = 1000 ppm, gas velocity = 0.556 m/s, [K$_2$CO$_3$] = 2 kmol m^{-3}).

Table 3
Experimental results for H$_2$S absorption

Inlet H$_2$S concentration (ppm)	Gas velocity (m s^{-1})	[K$_2$CO$_3$] (kmol m^{-3})	Outlet H$_2$S concentration (ppm) at $t=0$
1000	0.556	2.0	25.98
2071	0.556	2.0	43.00
1010	0.556	2.0	26.00
93	0.556	0.2	2.55
561	0.556	1.0	9.85
530	1.111	1.0	50.00
1000	1.111	2.0	100.00
2030	1.111	2.0	300.00
105	1.111	0.2	8.00

Table 4
Combined mass transfer coefficients

Gas velocity (m s^{-1})	Estimated k_{ext} (m s^{-1})	Used in simulation k_{ext} (m s^{-1})
0.556	1.62×10^{-2}	1.58×10^{-2}
1.111	1.70×10^{-2}	1.73×10^{-2}

of a module in the stack. However, during the experiment the liquid outlets of the each fiber were collected and were sent as a single inlet for next module, giving uniform concentrations at the inlet of all fibers. To get the similar effect in the simulation a hypothetical liquid mixing chamber was assumed at the outlet of each module. Similarly for the gas phase, in the actual module configuration a sufficient space was provided at junction point of the two modules. This void space acts a mixing chamber for the gas stream. Moreover, the modules were arranged in such a way that the fibers of the two consecutive modules were at right angles to each other. In such arrangements any concentration profile developed at the outlet of the shell side should vanish at the inlet of next module. Hence a complete mixing of the shell side flow at the outlet of each module was also assumed for simulation purpose. In the simulation, the combined mass transfer coefficient of the gas and the membrane phase was used as a fitting param-

eter. The estimated values of these combined mass transfer coefficient and the values used in the simulation are given in Table 4. It can be seen from Table 4 that both estimated and used values of the combined mass transfer coefficient match excellently.

The comparison of the experimental results and the simulation results are given in the form of parity plot in Fig. 10. It can be seen from this figure that there is a good match between the experimental results and numerical simulations.

7. Conclusion

In the present study, mass transfer with chemical reaction in a rectangular cross-flow membrane gas–liquid contactor is analyzed in detail. Two different experimental systems namely absorption carbon dioxide into aqueous carbonate solution and absorption of hydrogen sulphide in aqueous carbonate solution were used in the study. Experiments were carried out to study the effect of various operating parameters such as gas and liquid flow rates, concentrations of the feed streams and enhancement due to chemical reaction on the performance of the rectangular cross-flow membrane gas–liquid contactors.

Simple single gas permeation experiments were carried out to determine the membrane properties. The estimated value of ε/τ (=0.42) from these experiments for polypropylene Accurel Q3/2 hollow fibers is in good agreement with the value reported in literature data for this fiber (=0.36).

A detailed numerical model was developed to study mass transfer accompanied with chemical reaction in the cross-flow gas–liquid membrane contactor. The numerical model was solved for the detailed reaction schemes for the absorption of carbon dioxide and hydrogen sulphide into aqueous carbonate solution. The predictions of the numerical model are in good agreement with the experimental results. In case of the carbon dioxide absorption into aqueous carbonate solution, strong dependence of the absorption flux on the liquid velocity and relatively less dependence on the gas velocity indicates that mass transfer process is controlled by the liquid side mass transfer resistance. On the other hand, the combined resistance of the membrane and the gas phase is found to be dominant in the case of absorption of hydrogen sulphide in aqueous carbonate solution. The results in this work show that the detailed numerical model developed is able to predict the performance of the cross-flow membrane modules. The numerical simulation can take into account complex chemical reaction schemes. Thus the model can be used to predict the mass transfer performance of the cross-flow hollow fiber gas–liquid membrane contactor for other reactive as well as non-reactive systems simply by changing the physical and kinetic parameters. Furthermore, the model also represents a design and optimization tool for multi-component membrane gas absorption processes using cross-flow membrane modules.
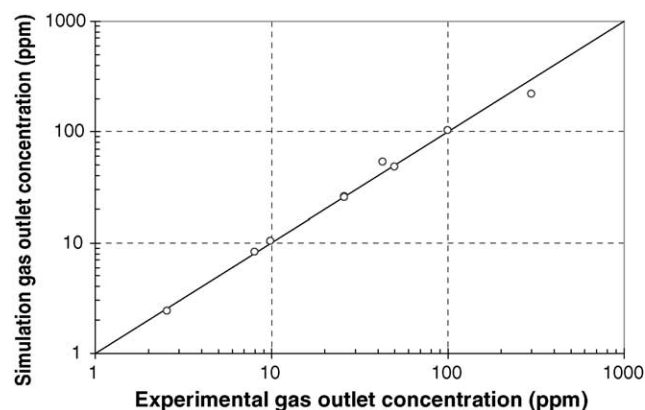

Fig. 10. Parity plot of predicted and experimental H$_2$S gas outlet concentration.

Acknowledgements

Nomenclature

A	area (m^2)
B_0	viscous flow parameter (m^2)
C	concentration ($mol\,m^{-3}$)
d	diameter (m)
D	diffusivity ($m^2\,s^{-1}$)
F	Faraday constant $= 96500$ ($C\,mol^{-1}$)
Gz	Graetz number, $\frac{vd^2}{Dz}$, (-)
J	flux ($mol\,m^{-2}\,s^{-1}$)
k	mass transfer coefficient ($m\,s^{-1}$)
$k_{sub,1}$	reaction rate constant, sub: reaction number, forward ($mol^{-1}\,m^3\,s^{-1}$)
$k_{sub,2}$	reaction rate constant, sub: reaction number, backward ($mol^{-1}\,m^3\,s^{-1}$)
K_{sub}	reaction equilibrium constant, sub: reaction number,
K_0	Knudsen flow parameter (m)
ℓ_i^∞	ionic conductivity at infinite dilution ($m^{-2}\,\Omega^{-1}\,mol^{-1}$)
L	length (m)
m	distribution coefficient (–)
M	molecular weight ($kg\,mol^{-1}$)
N	gas flux through membrane ($mol\,m^{-2}\,s^{-1}$)
P	pressure ($kg\,m^{-1}\,s^{-2}$)
Q	flow rate ($m^{-3}\,s^{-1}$)
r	radius (m)
R	gas constant ($J\,mol^{-1}\,K^{-1}$)
Re	Reynolds number, $\frac{dv\rho}{\mu}$, (-)
Sc	Schmidt number, $\frac{\mu}{\rho D}$, (-)
Sh	Sherwood number, $\frac{k_l d}{D}$, (-)
t	time (s)
T	temperature (K)
v	velocity ($m\,s^{-1}$)
z	length (m)
Z	ionic charge (–)

Greek letters

ε	porosity (–)
μ	viscosity ($kg\,m^{-1}\,s^{-1}$)
ρ	density ($kg\,m^{-3}$)
τ	tortuosity (–)

Subscripts/superscripts

avg	average
e	exit
ext	external
G	gas
i	inlet
i	component
in	inner
ini	initial
L	liquid
m	cell index
n	cell index
o	outer
p	pore
w	water
z	local value
∞	infinite dilution

Appendix A. Physico-chemical parameters

A.1. Solubility

The distribution coefficient of CO_2 in pure water was taken from Versteeg and van Swaaij [35].

$$m_{w,CO_2} = 3.59 \times 10^{-7} RT \exp\left(\frac{2044}{T}\right) \tag{A.1}$$

The distribution coefficient of H_2S in pure water was taken from Carroll and Mather [4].

$$m_{w,H_2S} = 1000 RT \times 10^{-a} \tag{A.2}$$

where,

$$a = 2.7896 + 0.031459\,T - 4.81046 \times 10^{-5}\,T^2$$
$$- \frac{672.791}{T} + 0.144237 \log T$$

The solubility of gas in aqueous electrolytic solutions was estimated using the method presented by Weisenberger and Schumpe [36]. The distribution coefficients for CO_2 and H_2S in aqueous solution of potassium carbonate were determined using Eqs. (A.3)–(A.5).

$$\log\left(\frac{m_{w,G}}{m_G}\right)$$
$$= (0.0959 + h_G)\,[K^+] + (0.0839 + h_G)[OH^-]$$
$$+ (0.0967 + h_G)[HCO_3^-] + (0.1423 + h_G)[CO_3^{-2}] \tag{A.3}$$

where the ionic concentrations are in $kmol\,m^{-3}$. h_G is the gas specific constant and is given for CO_2 and H_2S in following equations:

$$h_{CO_2} = -0.0172 - 3.38 \times 10^{-4}(T - 298.15) \tag{A.4}$$

$$h_{H_2S} = -0.0333 \tag{A.5}$$

A.2. Diffusivity

The diffusivity of CO_2 in pure water, D_{w,CO_2} was taken from Versteeg and van Swaaij [35].

$$D_{w,CO_2} = 2.35 \times 10^{-6} \exp\left(\frac{-2119}{T}\right) \tag{A.6}$$

The diffusivity of H_2S in pure water at 25 °C (2.10×10^{-9} m^2 s^{-1}) was taken from Diaz et al. [6]. The correction for the temperature and viscosity was carried out using the modified Stokes–Einstein relation presented by Versteeg and van Swaaij [35].

$$D\mu^{0.6} = \text{constant} \tag{A.7}$$

The diffusion coefficients of gases into aqueous electrolyte solutions were estimated by the method suggested by Ratcliff and Holdcroft [29].

$$\frac{D}{D_w} = 1 - (0.154[K_2CO_3] + 0.0723[KHCO_3]) \tag{A.8}$$

where concentrations are in kmol m^{-3}.

In case of the carbon dioxide absorption into carbonate solutions, ionic diffusion coefficients at infinite dilution were used. The ion diffusion coefficients at infinite dilution were estimated using the Nernst equation [18].

$$D_i^\infty = \ell_i^\infty \frac{RT}{z_i F^2} \tag{A.9}$$

The ionic conductivity at infinite dilution of various ions, ℓ_i^∞, was taken from the data available in Horvath [18]. In case of the hydrogen sulphide absorption into carbonate solution, the rate absorption is determined in whole or in part by the diffusion of carbonate ions to the reaction zone. The ionic diffusion of carbonate ions is influenced by the counter diffusion of bicarbonate and HS$^-$ ions. In this case mean effective diffusivity of ions was used for the calculation. The dependence of these diffusivities on the concentration of the carbonate solution was assumed to follow the modified Stokes–Einstein relation presented by Versteeg and van Swaaij [35].

A.3. Kinetic rate constants

An expression for the forward rate constant, $k_{1,1}$, as a function of co-electrolytes concentration was presented by Pohorecki and Moniuk [27].

$$\log \frac{k_{1,1}}{k_{1,1}^\infty} = 0.22\left(\frac{1}{2}[K^+]Z_{K^+}^2\right) + 0.22\left(\frac{1}{2}[OH^-]Z_{OH^-}^2\right)$$
$$+ 0.085\left(\frac{1}{2}[CO_3^{-2}]Z_{CO_3^{-2}}^2\right) \tag{A.10}$$

where $k_{1,1}^\infty$ (m^3 kmol^{-1} s^{-1}) is the rate constant for infinitely dilute solution.

$$\log k_{1,1}^\infty = 11.916 - \frac{2382}{T} \tag{A.11}$$

The effect of HCO$_3^-$ on the value of $k_{1,1}$ has not been reported, hence its influence on the forward rate constant was neglected.

Since the reactions (2) and (3) involve only proton transfer and can be considered as instantaneous, these reactions were assumed to be at equilibrium.

The reaction rate constant of the reaction of water with carbon dioxide, $k_{4,1}$, as a function of temperature is given by Sharma and Danckwerts [31]. The reaction is first order with respect to the concentration of the carbon dioxide.

$$\log k_{4,1} = 329.850 - 110.541 \log T - \frac{17265.4}{T} \tag{A.12}$$

The reaction of hydrogen sulphide with hydroxyl ion is a proton transfer reaction and can be considered as instantaneous one. The forward rate constant of reaction (11), $k_{5,1}$, has been measured to be 10^7 m^3 kmol^{-1} s^{-1} by Karmann [19] at 293 K. The information on the dependence of $k_{5,1}$ on the temperature was not mentioned.

A.4. Equilibrium constants

The equilibrium constant of the reaction (1), K_1 (m^3 kmol^{-1}), can be determined by the combination of the equilibrium for reaction (4) and reaction (3). The equilibrium constant for the reaction (2), K_2 (m^3 kmol^{-1}), at infinite dilution is reported by Hikita et al. [17].

$$\log K_2^\infty = \frac{1568.94}{T} + 0.4134 - 0.006737\,T \tag{A.13}$$

The effect of the electrolyte concentration on K_2 is given by Hikita et al. [17] and Roberts and Danckwerts [30].

$$\log \frac{K_2}{K_2^\infty} = \frac{1.01\sqrt{[K^+]}}{1 + 1.49\sqrt{[K^+]}} + 0.061[K^+] \tag{A.14}$$

The solubility product, K_w (kmol^2 m^{-6}), was taken from Tsonopolous et al. [33].

$$\log K_w = -\left(\frac{5839.5}{T} + 22.4773 \log T - 61.2062\right) \tag{A.15}$$

The equilibrium constant of reaction (4), K_4 (kmol m^{-3}) is reported in Sharma and Danckwerts [31].

$$\log K_4 = \frac{-3404.7}{T} + 14.843 - 0.03279\,T \tag{A.16}$$

The equilibrium constant of reaction (11) can be calculated from the first dissociation constant of hydrogen sulphide and ionic product of water. The first dissociation constant of hydrogen sulphide, K_a, is given by Tsonopolous et al. [33]

Table A.1
Parameters used for CO_2 absorption in aqueous K_2CO_3 solution at 297 K

Parameter	0.25 M	0.5 M
m	0.74	0.63
$k_{1,1}$ ($m^3\,kmol^{-1}\,s^{-1}$)	9.84×10^3	12.32×10^3
$k_{1,2}$ (s^{-1})	2.07×10^{-4}	2.54×10^{-4}
$k_{4,1}$ ($m^3\,kmol^{-1}\,s^{-1}$)	2.37×10^{-2}	2.37×10^{-2}
$k_{4,2}$ (s^{-1})	5.42×10^4	5.42×10^4
D_{CO_2} ($m^2\,s^{-1}$)	1.75×10^{-9}	1.64×10^{-9}
$D_{CO_3^{-2}}$ ($m^2\,s^{-1}$)	8.82×10^{-10}	8.42×10^{-10}
$D_{HCO_3^-}$ ($m^2\,s^{-1}$)	1.14×10^{-9}	1.01×10^{-9}
D_{OH^-} ($m^2\,s^{-1}$)	5.40×10^{-9}	5.15×10^{-9}

(Tables A.1 and A.2).

$$\log K_a = \frac{-5643.83}{T} - 33.5471 \log T + 94.9363 \quad \text{(A.17)}$$

Table A.2
Parameters used for H_2S absorption in aqueous K_2CO_3 solution at 293 K

Parameter	0.2 M	1 M	2 M
m	2.31	1.05	0.39
$K_{5,1}$ ($m^3\,kmol^{-1}\,s^{-1}$)	10^7	10^7	10^7
$K_{5,2}$ (s^{-1})	0.82	0.82	0.82
D_{H_2S} ($m^2\,s^{-1}$)	1.83×10^{-9}	1.60×10^{-9}	1.41×10^{-9}
D_{ion} ($m^2\,s^{-1}$)	1.12×10^{-9}	9.78×10^{-10}	8.62×10^{-10}

Appendix B. Characterization of the membrane for determination of the membrane mass transfer coefficient

B.1. Introduction

A membrane gas–liquid contactor offers several advantages over the conventional gas–liquid contactors. Improved performance can, however, only be realized, if the larger interfacial offered by membrane contactors is not compromised by the additional mass transfer resistance of the membrane. The membrane mass transfer coefficient can be determined through its structural properties such as thickness, pore size, porosity and tortuosity [7]. These membrane properties can be estimated easily for the membranes with uniform cylindrical pores. However, the assumption of uniform cylindrical pores is not valid for most of membrane structures. In this appendix, these membrane properties are determined for the microporous hollow fiber Accurel Q3/2 membranes using single gas permeation method [13].

B.2. Theory

The transport of a single gas through a porous membrane can be described by the dusty gas model. In case of the Accurel Q3/2 hollow fiber membrane the maximum pore size and average pore size according to the manufacturer's specification are 0.64 and 0.2 μm, respectively. These values are comparable to the mean free path of most of the gases at ambient conditions. Hence both Knudsen diffusion and vis-

cous flow will contribute to the total gas flow through the membrane pores according to Eq. (B.1).

$$N = -\frac{1}{RT}\left[K_0 V_m + B_0 \frac{P}{\mu}\right]\Delta P \quad \text{(B.1)}$$

where V_m is mean molecular velocity of the gas defined by Eq. (B.2)

$$V_m = \sqrt{\frac{8RT}{\pi M}} \quad \text{(B.2)}$$

K_0 and B_0 are the Knudsen diffusion and viscous flow morphology parameters of the membrane. For a homogeneous membrane K_0 and B_0 are membrane specific constants and independent of the permeating gas as long as no other gas-membrane interaction takes place (e.g. adsorption, surface diffusion). For membranes with uniform cylindrical pores K_0 and B_0 are given by Eq. (B.3)

$$K_0 = \frac{2\varepsilon r_p}{\tau}, \qquad B_0 = \frac{\varepsilon r_p^2}{8\tau} \quad \text{(B.3)}$$

where ε and τ are membrane porosity and tortuosity, respectively. Eq. (B.1) can be integrated over the membrane wall to give the outlet molar permeation flux. The final equation can be rearranged to get the membrane properties K_0 and B_0.

$$\frac{PQ_G \ln(r_o/r_{in})}{2\pi L \Delta P} = K_0 V_m + \frac{B_0}{\mu} P_{avg} \quad \text{(B.4)}$$

where P is shell side pressure, Q_G the volumetric permeation gas flux with respect to the outer membrane area, P_{avg} the arithmetic mean of the gas pressure at the inside and at the outside of the membrane fiber, ΔP the pressure difference between the inside and the outside of the membrane fiber. According to this equation K_0 and B_0 can be calculated from the slope and intercept of the plot of LHS of Eq. (B.4) versus P_{avg}.

B.3. Experimental

The single gas permeation experiments were carried out using Accurel Q3/2 microporous hollow fiber and nitrogen as a test gas. A schematic representation of the experimental set-up is given in Fig. B.1. A dead-end construction was chosen so that the entire flow was forced through the fiber. To ensure the constant pressure inside the fiber, small fiber length (3.6 cm) was used for the experiments. The gas flow from the cylinder was controlled using mass flow controller. Digital pressure transducers were used to measure the pressure inside and outside of the fiber. The average of three readings was taken for each individual measurement.

B.4. Results

The plot of LHS in Eq. (B.4) versus P_{avg} is shown in Fig. B.2. A good straight line correlation is obtained for the plot. The values of the membrane constant K_0 and B_0
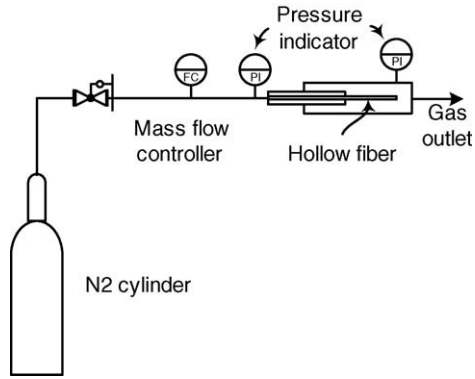
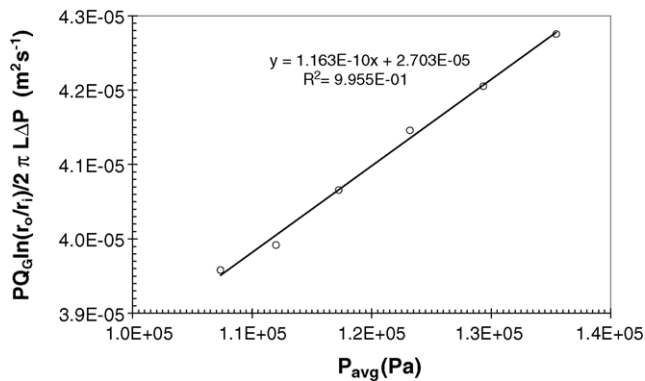Fig. B.1. Experimental set-up for the single gas permeation experiments.

Fig. B.2. Results for the single gas permeation experiments.

were calculated from the slope and the intercept of the plot ($K_0 = 4.23 \times 10^{-8}$ m, $B_0 = 2.12 \times 10^{-15}$ m^2). From these values, value of ε/τ (=0.42) was obtained for Accurel Q3/2 microporous hollow fiber. The estimated ε/τ value is in good agreement with the value estimated from the literature data; $\varepsilon/\tau = 0.36$ [13].

References

[1] G. Astarita, F. Gioia, Hydrogen sulphide chemical absorption, Chem. Eng. Sci. 19 (1964) 963–971.

[2] G. Astarita, Mass Transfer with Chemical Reaction, Elsevier, Amsterdam, 1967.

[3] G.A. Baker, T.A. Oliphant, An implicit numerical method for solving the two dimensional heat equation, Quart. Appl. Math. 17 (4) (1960) 361–373.

[4] J.J. Carroll, A.E. Mather, The solubility of hydrogen sulphide in water from 0 to 90 °C and pressure to 1 MPa, Geochim. Cosmochim. Acta 53 (1989) 1163–1170.

[5] M. Chun, K. Lee, Analysis on a hydrophobic hollow fiber membrane absorber and experimental observations of CO$_2$ removal by enhanced absorption, Sep. Sci. Technol. 32 (15) (1997) 2445–2466.

[6] D. Diaz, A. Vega, J. Coca, Correlation for the estimation of gas–liquid diffusivity, Chem. Eng. Commun. 52 (1987) 271–281.

[7] V.Y. Dindore, D.W.F. Brilman, F.H. Geuzebroek, G.F. Versteeg, Membrane-solvent selection for CO$_2$ removal using membrane gas–liquid contactors, Sep. Purif. Technol. 40 (2004) 133–145.

[8] V.Y. Dindore, D.W.F. Brilman, G.F. Versteeg, Cross flow gas–liquid membrane contactors: physical mass transfer processes, J. Membr. Sci. (2005) in press.

[9] V.Y. Dindore, D.W.F. Brilman, G.F. Versteeg, Shell-side dispersion coefficients in a rectangular cross-flow hollow fiber membrane module, Chem. Eng. Res. Design 83 (A3) (2005) 1–9.

[10] L.K. Doraiswamy, M.M. Sharma, Heterogeneous Reactions: Analysis, Examples, and Reactor Design. Fluid-Fluid-Solid Reactions, vol. 2, Wiley, Singapore, 1984.

[11] V.Y. Dindore, D.W.F. Brilman, P.H.M. Feron, G.F. Versteeg, CO$_2$ absorption at elevated pressures using a hollow fiber membrane contactor, J. Membr. Sci. 235 (1–2) (2004) 99–109.

[12] L. Graetz, Über die Wärmeleitungsfähigkeit von Flüssigkeiten, 1e Abhandlung, Annalen der Physik und Chemie 18 (1883) 79–84.

[13] C.S. Guijt, I.G. Racz, T. Reith, A.B. de Haan, Determination of membrane properties for use in the modeling of a membrane distillation module, Desalination 132 (2000) 255–261.

[14] A.E. Jansen, R. Klaassen, P.H.M. Feron, J.H. Hanemaaijer, B.Ph. ter Meulen, Membrane gas absorption processes in environmental applications, in: J.G. Crespo, K.W. Boddeker (Eds.), Membrane Processes in Separation and Purification, Kluwer Academic Publishers, Dordrecht, 1994, pp. 343–356.

[15] P.H.M. Feron, A.E. Jansen, Capture of carbon-dioxide using membrane gas-absorption and reuse in the horticultural industry, Energy Convers. Manage. 36 (69) (1995) 411–414.

[16] C. Hanisch, Exploring options for CO$_2$ capture and management, Environ. Sci. Technol. 33 (3) (1999) 66A–70A.

[17] H. Hikita, S. Asai, T. Takatsuka, Absorption of carbon dioxide into aqueous sodium hydroxide and sodium carbonate and bicarbonate solutions, Chem. Eng. J. 11 (1976) 131–141.

[18] A.L. Hovarth, Handbook of Aqueous Electrolytic Solutions: Physical Properties, Estimation and Correlation Methods, Wiley, New York, 1985.

[19] W. Karmann, Pulse radiolysis of H$_2$S in aqueous solution, Naturforsh B22 (3) (1967) 273.

[20] H. Kreulen, C.A. Smolders, G.F. Versteeg, W.P.M. van Swaaij, Microporous hollow-fiber membrane modules as gas–liquid contactors: 1. Physical mass transfer processes—a specific application: mass transfer in highly viscous liquids, J. Membr. Sci. 78 (3) (1993) 197–216.

[21] P.S. Kumar, Development and design of membrane gas absorption processes, PhD Thesis, University of Twente, The Netherlands, 2002.

[22] Y. Lee, R.D. Noble, B. Yeom, Y. Park, K. Lee, Analysis of CO$_2$ removal by hollow fiber membrane contactors, J. Membr. Sci. 194 (2001) 57–67.

[23] J. Leveque, Les lois de la transmission de chaleur par convection (series 12), Annls. Mines, Paris, 1928, p. 201.

[24] S. Nii, H. Takeuchi, K. Takahashi, Removal of CO$_2$ by gas absorption across a polymeric membrane, J. Chem. Eng. Jpn. 25 (1) (1992) 67–71.

[25] R.A.T.O. Nijsing, R.H. Hendriksz, H. Kramers, Absorption of CO$_2$ in jets and falling films of electrolyte solutions, with and without chemical reaction, Chem. Eng. Sci. 10 (1959) 88–104.

[26] R.H. Perry, D. Green, Perry's Chemical Engineer's Handbook, McGraw-Hill, Singapore, 1984.

[27] R. Pohorecki, W. Moniuk, Kinetics of the reaction between carbon dioxide and hydroxyl ion in aqueous electrolyte solutions, Chem. Eng. Sci. 43 (1988) 1677–1684.

[28] Z. Qi, E.L. Cussler, Microporous hollow fibers for gas absorption. II. Mass transfer across the membrane, J. Membr. Sci. 23 (1985) 333–345.

[29] G.A. Ratcliff, J.G. Holdcroft, Diffusivities of gases in aqueous electrolyte solutions, Trans. Inst. Chem. Eng. 41 (1963) 315–319.

[30] D. Roberts, P.V. Danckwerts, Kinetics of CO$_2$ in alkaline solution–I, Chem. Eng. Sci. 17 (1967) 961–969.

[31] M.M. Sharma, P.V. Danckwerts, The absorption of carbon dioxide into solutions of alkalis and amines (with some notes on hydro-

gen sulphide and carbonyl sulphide), Chem. Eng. (1966) CE245–CE280.

[32] W. Strauss, Industrial Gas Cleaning, Pergamon Press, Oxford, 1975.

[33] C. Tsonopolous, D.M. Coulson, L.W. Inman, Ionization constants of water pollutants, J. Chem. Eng. Data 21 (1976) 190–193.

[34] R.D. Vas Bhat, J.A.M. Kuipers, G.F. Versteeg, Mass transfer with complex chemical reactions in gas–liquid systems: two-step reversible reactions with unit stoichiometric and kinetic orders, Chem. Eng. J. 76 (2) (2000) 127–152.

[35] G.F. Versteeg, W.P.M. van Swaaij, Solubility and diffusivity of acid gases (CO_2, N_2O) in aqueous alkanolamine solutions, J. Chem. Eng. Data 33 (1988) 29–34.

[36] S. Weisenberger, A. Schumpe, Estimation of gas solubility in salt solutions at temperatures from 273 K to 363 K, AIChE J. 42 (1) (1996) 298–300.